JCTC Journal of Chemical Theory and Computation

Article

pubs.acs.org/JCTC

Application of Automated Reaction Path Search Methods to a Systematic Search of Single-Bond Activation Pathways Catalyzed by Small Metal Clusters: A Case Study on H−H Activation by Gold

Min Gao,[†] Andrey Lyalin,[‡,§] Satoshi Maeda,*[,†,‡] and Tetsuya Taketsugu[†,‡]

[†]Department of Chemistry, Faculty of Science, Hokkaido University, Sapporo 060-0810, Japan

[‡]Elements Strategy Initiative for Catalysts and Batteries (ESICB), Kyoto University, Kyoto 615-8245, Japan

Supporting Information

ABSTRACT: A new theoretical approach to find metal-cluster-catalyzed single bond activation pathways is introduced. The proposed approach combines two automated reaction path search techniques: the anharmonic downward distortion following (ADDF) and the artificial force induced reaction (AFIR) methods, developed in our previous works [Maeda, S.; Ohno, K.; Morokuma, K. *Phys. Chem. Chem. Phys.* **2013**, *15*, 3683−3701]. A simple model reaction of the H−H bond activation catalyzed by Au_n (n = 7, 8) clusters is considered as an example. We have automatically found 33 and 20 transition-state (TS) structures for H_2 dissociation on Au_7 and Au_8 clusters, respectively, and successfully identified the best dissociation pathways with the lowest barrier. Systematic analysis of the structure-dependent reactivity of small gold clusters is performed. It is demonstrated that the most stable structures of the gold clusters are not always highly reactive and several isomeric structures must be taken into account for adequate description of the reaction rates at finite temperatures. The proposed approach can serve as a promising tool for investigation of the chemical reactions catalyzed by small metal clusters.

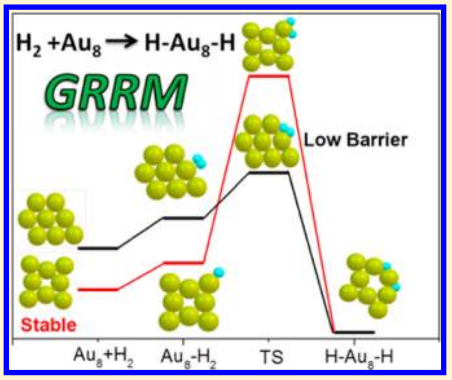

1. INTRODUCTION

Catalysis by nanoscaled particles (nanocatalysis) is one of the most exciting fields of modern nanoscience.[1] The enormous interest in nanocatalysis is stipulated by the fact that the catalytic activity of nanoparticles is strongly dependent on their size, structure, morphology, charge state, type of the support material, etc., and hence can be controlled and tuned by these factors. Even clusters of the same size, but with different geometrical structure, can possess different reactivity. However, despite intensive theoretical and experimental studies, the clear understanding of the morphology effects in nanocatalysis is still lacking. The present work fills this gap on the example of small clusters of gold. Gold is one of the most studied metals in nanocatalysis, because of its unique catalytic properties emerging at nanoscale.[2−5] Moreover, gold nanoparticles demonstrate extraordinary catalytic activity and selectivity, even at room temperature,[5−9] which is very attractive for industrial and chemical applications.

Gold clusters can possess various structures ranging from the one-dimensional (1D) nanowires to the planar (2D), the three-dimensional (3D), and even the cagelike structures.[10−14] Theoretical investigations on structure of gold clusters have been performed using various global optimization techniques and/or local geometry optimizations.[15−17] A large number of chemical reactions catalyzed by the gold clusters have also been investigated theoretically.[12,18−24] Among these studies, the subject of H_2 activation and dissociation is of particular interest, because of its importance for industrial hydrogenation processes. Several factors, such as cluster size, coordination of the adsorption site, cluster charge, etc., can influence H−H bond activation upon H_2 adsorption on gold clusters.[25−31] Many theoretical studies on the reactivity of cluster consider only the most stable geometric structures as an effective (or representative) catalyst. This is, in part, a reasonable approach, because the most stable structure often has the highest population in the ensemble of clusters at finite temperature. However, it has been shown that gold nanoparticles possessing many isomeric structures and lying in a close energy range can be fluxional at room temperature on a time scale of a few tens of picoseconds.[32−37] Such a fluxionality occurs at the typical time scale of chemical reactions. Therefore, it is rather questionable to consider only the most stable structures for description of the reactivity of cluster at finite temperatures.

Systematic studies on structural dependence of the catalytic activity of gold clusters of a given size have been scarce, despite its significance for adequate description of various chemical processes on a cluster surface. To accomplish this, an exhaustive search of pathways for the catalytic reactions occurring not only on the most stable cluster structure but also on the low-energy isomeric structures is required. In particular, in order to describe the H−H bond activation by a gold cluster Au_n

Received: January 29, 2014
Published: March 13, 2014

   dx.doi.org/10.1021/ct500068b | *J. Chem. Theory Comput.* 2014, 10, 1623−1630

correctly, massive calculations consisting of the following three stages are needed:

(1) collect all low-lying local minimum structures for the Au_n cluster;
(2) find all low-barrier H−H bond dissociation pathways on the isomeric structures obtained in stage (1); and
(3) explore relaxation pathways for the Au_nH_2 clusters obtained in stage (2).

For stage (1), many efficient global optimization methods are available.[38,39] However, in most previous studies, the reaction pathways have usually been determined one-by-one via conventional geometry optimization techniques. Since the systematic search of reaction paths by geometry optimizations is a difficult task, only a few isomers have usually been considered as representative catalysts.

There have been considerable efforts on development of automated reaction path search methods.[40−51] Application of these methods to the above problem would be a subject of great interest for systematic analysis and prediction of reactivity of small metal clusters. In the present study, we propose a novel effective strategy for a systematic search of the best pathway for single bond activation reactions on gold clusters. In order to perform the above three-stage calculations, the present approach combines two automated reaction path search methods: the anharmonic downward distortion following[51−54] (ADDF) method and the artificial force induced reaction[51,55,56] (AFIR) method. The ADDF method can be used to explore reaction pathways of A → X (+ Y) type automatically starting from a local minimum A to its isomer X or dissociated fragments X + Y, which is employed in stages (1) and (3). The AFIR method can be used for the efficient automatic search of reaction pathways of the A + B → X (+ Y) type starting from the separated fragments A + B, which is employed at stage (2). Thus, the above three-stage calculations can be performed by the present strategy. The present approach was applied to the H−H bond activation on small gold clusters, Au_7 and Au_8.

2. METHODS

2.1. ADDF Method. The ADDF method has been developed to explore reaction pathways automatically, starting from local minima on quantum chemical potential energy surfaces. Along typical reaction paths, curvature of the potential energy curve changes smoothly from positive to negative through the course of moving from a local minimum to a transition state (TS). In other words, slopes of the potential curve should always decline from their respective harmonic curves because of energy-lowering interactions that lead to a TS. Hence, the ADDF method searches for TSs by proceeding to directions showing maximal anharmonic downward distortion (ADD). Once a TS is found, the intrinsic reaction coordinate (IRC)[57] is calculated to determine the next local minimum to which the TS connects. In the standard algorithm, all possible ADD-maximal pathways are followed, starting from all obtained local minima, and a full network of reaction pathways can be obtained. This has been done for ground-state molecules consisting of ∼10 atoms, but would become very expensive for larger molecules. In many applications, high-energy structures are not required. In such cases, one can use the large ADD following algorithm, in which only the largest n ADD directions are considered. Additional details have been described in a recent review.[51]

2.2. AFIR Method. In the AFIR method, two (or more) fragments are pushed together, by minimizing a model function called the AFIR function. The AFIR function $F(\mathbf{Q})$ is composed of the adiabatic PES $E(\mathbf{Q})$ and an artificial force term.[51,55,56]

$$F(\mathbf{Q}) = E(\mathbf{Q}) + \alpha\frac{\sum_{i\in A}\sum_{j\in B}\omega_{ij}r_{ij}}{\sum_{i\in A}\sum_{j\in B}\omega_{ij}} \quad (1)$$

In eq 1, summation of the distance r_{ij} between atoms i and j in fragments A and B, respectively, is taken with weight ω_{ij}. This weight function ω_{ij} is chosen to be

$$\omega_{ij} = \left[\frac{(R_i + R_j)}{r_{ij}}\right]^p \quad (2)$$

In this equation, R_i is the covalent radius for atom i, and p is set to the standard value of 6. For the convenience of the users, α can be rewritten as follows:

$$\alpha = \frac{\gamma}{\left[2^{-1/6} - \left(1 + \sqrt{1 + \frac{\gamma}{\varepsilon}}\right)^{-1/6}\right]R_0} \quad (3)$$

The model collision energy parameter γ is introduced in eq 3, and, in this equation, α corresponds to the mean force that acts between two Ar atoms on the Lennard-Jones potential (R_0 = 3.8164 Å and ε = 1.0061 kJ/mol) from the minimum point to the turning point in their direct collision with collision energy γ. In other words, γ provides an approximate upper limit of the barrier height to be searched. In the standard algorithm for bimolecular and multicomponent reactions, initially, given fragments (Au_n and H_2 in the present case) are randomly placed, and then the AFIR function of eq 1 is minimized. The path of minimization of the AFIR function is called the AFIR path. An AFIR minimization gives an approximate product structure as a local minimum on the AFIR function, when γ is sufficiently large to overcome the barrier. The maximum point for $E(\mathbf{Q})$ along the AFIR path can be an approximate TS geometry. The accurate product and TS geometries are then fully optimized without artificial force from these approximate structures using any standard optimization method. By repetition of minimization of the AFIR function starting from a sufficient number of random geometries, associative pathways can be sampled between given reactants. Additional details also have been described in a recent review.[51]

2.3. The Present Strategy. The proposed approach consists of the following five steps:

(i) search for low-lying isomers of Au_n clusters by the ADDF method;
(ii) search of approximate reaction paths (AFIR paths) for reactions between H_2 and low-lying isomers of Au_n cluster obtained in step (i) by the AFIR method;
(iii) reoptimization of the AFIR paths obtained in step (ii) by a conventional path optimization method, the locally updated plane (LUP) method,[58] without artificial force;
(iv) optimization of the transition-state (TS) structures for the H−H bond dissociation, starting from the maximum energy points along the paths of the LUP method obtained in step (iii), by the rational function optimization[59] (RFO) method (note that, for the TSs obtained, normal-mode analysis and the intrinsic reaction coordinate (IRC) calculations were performed); and
(v) search for relaxation paths of Au_nH_2 clusters to its more stable forms by the ADDF method, starting from an intermediate that is generated through the best path for the H−H bond dissociation step obtained in step (iv).

In step (ii), only isomeric structures lying in the energy range of 20 kJ/mol, relative to the most stable one, have been selected for further investigations of reactions with H_2. This is because the typical barrier heights of low-lying paths for the H−H bond dissociation step are ∼20−30 kJ/mol, and, hence, contributions from the energetically higher-lying isomers are negligible. In this selection of isomers, relative energy values with 12 different conditions, i.e., electronic energy with and without the zero-point-energy correction and Gibbs free energy at 298.15 × m/10 (m = 1, 2, ..., 10) K, were considered, in order to obtain results at various temperatures by a single calculation, where this setting has been adopted in our previous studies on H-bond

dx.doi.org/10.1021/ct500068b | J. Chem. Theory Comput. 2014, 10, 1623−1630

clusters[60] inspired by the parallel tempering Monte Carlo simulations.[61]

This five-step calculation gives a multistep reaction path starting from H_2 + Au_n to a stable form of the Au_nH_2 clusters through TS with the lowest H−H bond activation barrier. All required codes for ADDF,[51−54] AFIR,[51,55,56] LUP,[58] RFO,[59] and IRC[62] calculations are available in a developmental version of the GRRM (Global Reaction Route Mapping) program,[51] and such multistep paths can be obtained automatically with a simple script to execute these calculations sequentially. Details of employed parameters and density functional theory (DFT) calculations are described below.

2.4. Search Parameters. In step (i), calculations of TS and IRC were not performed in order to explore only local minima efficiently, although ADDF can locate local minima as well as TSs and IRCs. The ADDF searches were started from n random structures, where n is the number of Au atoms. The large-ADDF option was employed, and the five largest ADD paths were followed to locate the five lowest isomerization pathways starting from each local minimum. The ADDF procedure was applied to the n lowest minima in terms of electronic energy with and without the zero-point-energy correction and free energy at 298.15 × m/10 (m = 1−10) K. The set of parameters discussed here is identical to those employed in our previous studies on hydrogen-bond clusters.[60]

Step (i) generates a list of cluster isomers. From the list, all cluster isomers with a relative energy (in terms of electronic energy with and without the zero-point-energy correction and free energy at 298.15 × m/10 (m = 1−10) K) of <20 kJ/mol, compared to the lowest one, were chosen, and they were reacted with H_2 in step (ii). Starting from random orientations and directions between the selected isomers of Au clusters and H_2, they were pushed together by artificial force until a reaction occurred. In this study, a specific force is applied to accelerate the H_2 dissociation path searches: a positive force between gold clusters and each H atom and a negative force between H atoms. Precisely, the AFIR function in eq 1 is modified as follows:

$$F(\mathbf{Q}) = E(\mathbf{Q}) + \frac{\alpha}{3}\left(\frac{\sum_{i\in A}\omega_{iB}r_{iB}}{\sum_{i\in A}\omega_{iB}} + \frac{\sum_{i\in A}\omega_{iC}r_{iC}}{\sum_{i\in A}\omega_{iC}} - r_{BC}\right) \quad (4)$$

In this equation, A corresponds to the Au_n cluster and B and C are the two H atoms in H_2, α is given in eq 3, $\omega_{iB/C}$ can be computed by eq 2 for the ith Au atom and H atom (B or C), $r_{iB/C}$ is the distance between the ith Au atom and H atom (B or C), and r_{BC} is the distance between the two H atoms. This treatment leads the AFIR paths directly to the H−H bond dissociation TSs, avoiding useless calculations in the adsorption state of H_2 on Au_n clusters, and a similar strategy would be useful for other single-bond activation reactions such as C−H activations. This stochastic path sampling was terminated when successive x path calculations located no new intermediate structure, where x = 30 was applied in this study. For the most stable Au_7 isomer, x = 100 was tested, and it was found that x = 30 is sufficient to locate the best pathway for H_2 dissociation. The model collision-energy parameter γ in eq 3 restricts the upper-limit of barrier height to be found to ∼γ. In this study, γ values of 100 kJ/mol and 300 kJ/mol were considered for these tests.

The step (ii) samples approximate reaction paths called AFIR paths, which have been shown to resemble IRC paths.[51,55,56] These AFIR paths were reoptimized in step (iii) via a path-optimization method, locally updated plane (LUP) method.[58] Although LUP calculations starting from linear interpolation require massive iterations, AFIR paths are already close to IRC paths and only five iterations were taken. Then, in step (iv), maximum energy points along these paths were collected and TS structures were identified by a standard quasi-Newton method. Finally, all TSs and their connections were confirmed by normal-mode and IRC calculations.

In step (v), relaxation paths of the Au_nH_2 clusters were searched by the ADDF method, starting from an intermediate that is generated through the best path for the H−H bond dissociation step. The large-ADDF option was employed,[60] and the three largest ADD paths were followed to locate the three lowest isomerization pathways starting from each local minimum. The ADDF procedure was applied to the three lowest minima, in terms of electronic energy with and without the zero-point-energy correction and free energy at 298.15 × m/10 (m = 1−10) K.

2.5. DFT Calculation. In the present study, all the reaction-path search calculations were done by a local developmental version of the GRRM program. In the search, potential energy gradients are required. In this study, gradients were computed on the basis of DFT with the PBE functional,[63] using the SIESTA program.[64−66] The PBE functional has been reported to be a good density functional for the simulation of gold clusters.[67] It has been successfully used to describe isomers of gold clusters and H_2 dissociation on TiO_2-supported gold clusters in our recent research.[29] Double-ζ plus polarization function (DZP) basis sets are used to treat the $1s^1$ and $6s^15d^{10}$ valence electrons of H and Au atoms, respectively.[68] The core electrons for Au atoms are represented by the Troullier−Martins norm-conserving pseudopotentials.[69] An energy cutoff of 100 Ry is chosen to guarantee convergence of total energies and forces. A common energy shift of 50 meV is applied. We note that this is the first time to combine GRRM with SIESTA, and the GRRM/SIESTA approach can be a very powerful tool to investigate catalysis and the material chemistry by DFT and the automated reaction path search methods.

3. RESULTS AND DISCUSSION

Let us denote the ith energetically low-lying isomer of the gold cluster Au_n as $C_{n,i}$, where i = 0 corresponds to the most stable structure. From step (i), 11 and 18 isomers have been located for Au_7 and Au_8 clusters, respectively. The highest-energy isomer $C_{7,11}$ was found in step (iv) by reoptimization of the terminal point of the IRC path without H_2. All the geometries are listed in Figure 1 with their relative energy values. Many works[32,67,70−77] have been done to investigate the stability and structure of gold clusters, and the PBE functional employed in this study has been reported to give reasonable results for gold clusters.[67] It has been shown that the gold clusters are planar when the size is smaller than Au_7. The most stable isomer of Au_7, $C_{7,0}$, has a planar structure, which is consistent with the experimental observations performed in the gas phase;[32] it is also consistent with the previous theoretical calculations.[70−73] The difference in free energy between the second-lowest structure of the Au_7 cluster ($C_{7,1}$) and the most stable structure of the Au_7 cluster ($C_{7,0}$) is calculated to be 14.7 kJ/mol. Concerning the most stable structure of Au_8, there have been arguments about whether it is planar or not.[67,74−76] The lowest $C_{8,0}$ structure in Figure 1 is planar, which is consistent with some DFT results,[11,77] as well as with very recent CCSD(T) calculations.[74,76] Moreover, relative electronic energies of the $C_{8,2}$ and $C_{8,3}$ structures, relative to the most stable $C_{8,0}$ structure, 16.4 and 17.1 kJ/mol, respectively, are close to the results by CCSD(T)/cc-pVTZ-pp+CV calculations (19.2 and 18.4 kJ/mol).[76] The present PBE calculation well reproduces both experimental[32] and high-level ab initio results.[76]

Figure 2a shows free energy profiles along all obtained H_2 dissociation paths on low-lying Au_7 isomers, where $A_{7,i,j}$ corresponds to the jth lowest adsorption state between $C_{7,i}$ and H_2, $TS_{7,i,j}$ is the TS for the IRC path connected to $A_{7,i,j}$, $IM_{7,i,j}$ is the intermediate generated through the IRC path starting from $TS_{7,i,j}$, and $P_{7,i,j}$ corresponds to the IRC path through $TS_{7,i,j}$. Free-energy values are calculated relative to $C_{7,0}$ + H_2 (sum of free energy values for separately optimized $C_{7,0}$ and H_2). Among 12 isomers of Au_7 clusters shown in Figure 1a, the lowest four, $C_{7,0}$, $C_{7,1}$, $C_{7,2}$, and $C_{7,3}$, were considered for further reaction with H_2 since these structures satisfy the energy-based selection criteria explained above. In Figure 2a, some higher lying paths connected to the high-energy isomers, $C_{7,4}$, $C_{7,7}$, $C_{7,8}$, and $C_{7,11}$, are also shown to demonstrate the

dx.doi.org/10.1021/ct500068b | J. Chem. Theory Comput. 2014, 10, 1623−1630

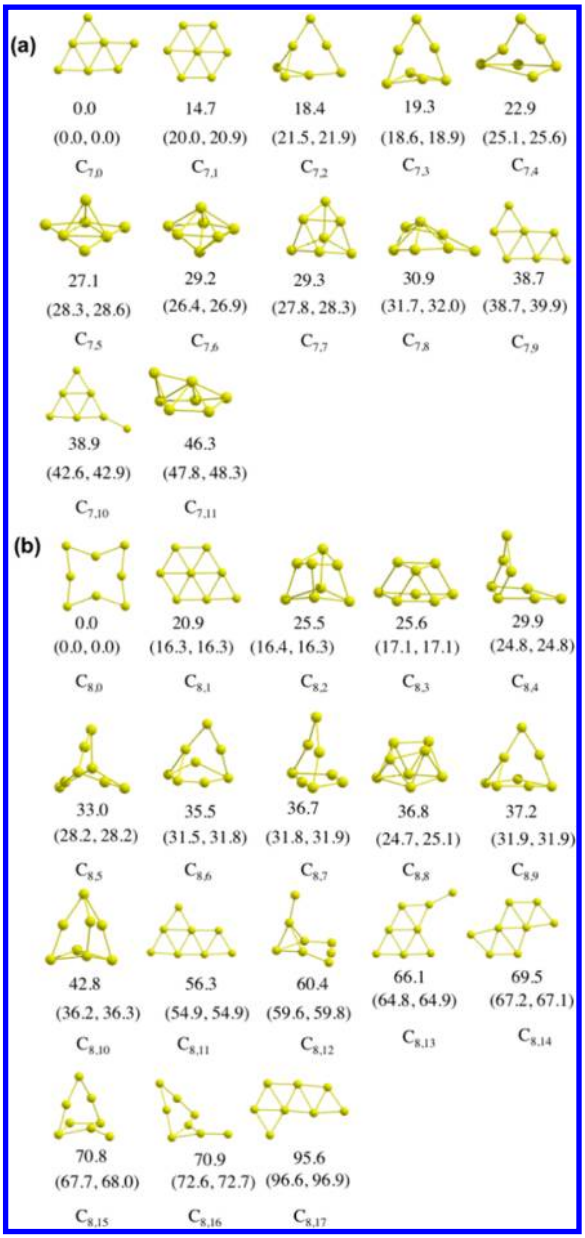

Figure 1. (a) Optimized geometries of Au_7 clusters labeled as $C_{7,i}$ and (b) those of Au_8 clusters labeled as $C_{8,i}$. Free-energy values (298.15 K, 1 atm), relative to the most stable structures ($C_{7,0}$ and $C_{8,0}$) are shown below each structure. Isomer $C_{7,11}$ was found in step (iv) rather than step (i) (see text for details). Relative electronic energy values without and with zero-point energy corrections are given in parentheses. All energy values are given in terms of kJ/mol. Cartesian coordinates for all these structures are available in the Supporting Information.

large structural rearrangements during path searches by the AFIR method.

It should be noted that the relative importance of each path can be analyzed on the basis of the relative free-energy values of $TS_{7,i,j}$. The reaction rate passing $P_{7,i,j}$ from $C_{7,i} + H_2$ to $IM_{7,i,j}$ can be written as $k_{ij}[C_{7,i}][H_2]$, where $[C_{7,i}]$ and $[H_2]$ are the concentrations of $C_{7,i}$ and H_2, respectively. The rate constant k_{ij} can be estimated by the transition-state theory (TST) as

$$k_{ij} = \left(\frac{k_B T}{h}\right) \exp -\left[\frac{(\Delta G[TS_{7,i,j}] - \Delta G[C_{7,i} + H_2])}{RT}\right] \quad (5)$$

where k_B is the Boltzmann constant, T the temperature, h Planck's constant, $\Delta G[TS_{7,i,j}]$ the relative free energy of $TS_{7,i,j}$, $\Delta G[C_{7,i} + H_2]$ the relative free energy of $C_{7,i} + H_2$, and R the gas constant. Assuming thermal equilibrium among Au_7 isomers, $[C_{7,i}]$ is proportional to the Boltzmann factor, i.e.,

$$[C_{7,i}] \propto \exp\left[-\frac{(\Delta G[C_{7,i}] - \Delta G[C_{7,0}])}{RT}\right] \quad (6)$$

where $\Delta G[C_{7,i}]$ is the relative free energy of $C_{7,i}$ ($\Delta G[C_{7,i}] = \Delta G[C_{7,i} + H_2]$), and $\Delta G[C_{7,0}] = 0$. Thus, the reaction rate $k_{ij}[C_{7,i}][H_2]$ passing $P_{7,i,j}$ is proportional to the product of $\exp[-\Delta G[TS_{7,i,j}]/RT]$ and $[H_2]$. Therefore, it means that the relative importance of each path can be discussed just by comparing the $\Delta G[TS_{7,i,j}]$ values. Although there may be some other approaches, in this study, we adopt the Boltzmann distribution among Au cluster isomers and the conventional TST to evaluate the relative importance of each path.

In the case of Au_7, totally 33 paths were obtained for the H_2 dissociation. Although relative *electronic energy* values of $A_{7,i,j}$ are negative, their relative *free energy* values calculated for the room-temperature conditions (T = 298.15 K) are all positive, as seen in Figure 2a, because the system is destabilized due to the entropy loss by the H_2 adsorption to Au_7 clusters. Furthermore, $P_{7,0,0}$, starting from the most stable adsorption structure $A_{7,0,0}$, has a pretty high barrier (also see Figure 2b for their geometries), indicating that stability of adsorption structures $A_{7,i,j}$ does not correlate to the corresponding barrier height for $TS_{7,i,j}$. In $A_{7,0,0}$, the H_2 binding energy $E^b_{7,0,0}$ (i.e., $E^b_{7,0,0} = E(C_{7,0}) + E(H_2) - E(A_{7,0,0})$), in terms of electronic energy plus zero-point energy is 11.1 kJ/mol, the Au−H distances are 2.08/2.08 Å, and the H−H distance is 0.78 Å. In $TS_{7,0,0}$, the H−H distance is increased to 1.97 Å, and, finally, the H−H bond is dissociated in $IM_{7,0,0}$. In Figure 2c, the three lowest pathways $P_{7,0,2}$, $P_{7,1,0}$, and $P_{7,1,1}$ are shown. At $A_{7,0,2}$, $A_{7,1,0}$, and $A_{7,1,1}$, the H_2 binding energies $E^b_{7,0,2}$, $E^b_{7,1,0}$, and $E^b_{7,1,1}$ are 10.8, 22.1, and 22.1 kJ/mol, and the Au−H distances are 1.96/2.00, 1.90/1.91, and 1.90/1.90 Å, respectively. In these low-lying paths, the H−H distance is substantially elongated at $A_{7,0,2}$, $A_{7,1,0}$, and $A_{7,1,1}$ to 0.80, 0.82, and 0.82 Å, respectively, compared to 0.78 Å of $A_{7,0,0}$ as well as 0.74 Å of isolated H_2 molecules. Moreover, $TS_{7,0,2}$, $TS_{7,1,0}$, and $TS_{7,1,1}$, with short H−H distances 1.38, 1.34, and 1.21 Å, respectively, are early TSs. These structural features are consistent with the high reactivity of $P_{7,0,2}$, $P_{7,1,0}$, and $P_{7,1,1}$. These three have similar barriers and may compete with each other. Actually, the rate factor $\exp[-\Delta G[TS_{7,i,j}]/RT]$ for $P_{7,0,2}$, $P_{7,1,0}$, and $P_{7,1,1}$ are 2.3×10^{-9}, 1.5×10^{-9}, and 0.4×10^{-9}, respectively. Since the contributions of the higher barrier paths are negligible, the lowest cluster isomer $C_{7,0}$ accounts for ~55% of the total rate. The remaining 45% are assigned to the sum of those for $P_{7,1,0}$, and $P_{7,1,1}$, starting from the second lowest isomer $C_{7,1}$. In this system, three paths starting from the different isomer and adsorption structures are competing. This result demonstrates the significance of the systematic search for reaction pathways.

Figure 3 shows the results for the Au_8 clusters, where $A_{8,i,j}$ corresponds to the jth lowest adsorption state between $C_{8,i}$ and H_2, $TS_{8,i,j}$ is the TS for the IRC path connected to $A_{8,i,j}$, $IM_{8,i,j}$ is the intermediate generated through the IRC path starting from $TS_{8,i,j}$, and $P_{8,i,j}$ corresponds to the IRC path through $TS_{8,i,j}$. Free-energy values are calculated relatively to $C_{8,0} + H_2$ (sum of free-energy values for separately optimized $C_{8,0}$ and H_2). Among 13 isomers of Au_8 clusters shown in Figure 1b, the

dx.doi.org/10.1021/ct500068b | J. Chem. Theory Comput. 2014, 10, 1623−1630

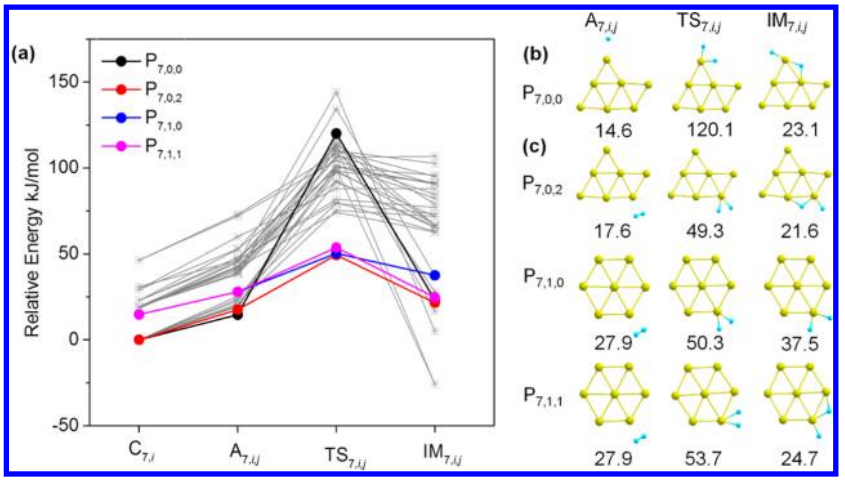

Figure 2. (a) Free-energy profiles (298.15 K, 1 atm) along 33 IRC paths calculated for H_2 dissociation on several isomeric structures of Au_7. Free-energy values are calculated relatively to the sum of the free energies of the most stable Au_7 structure ($C_{7,0}$) and the free H_2 molecule. $A_{7,i,j}$ corresponds to the *j*th lowest adsorption state between $C_{7,i}$ and H_2; $TS_{7,i,j}$ is the TS for the IRC path connected to $A_{7,i,j}$; $IM_{7,i,j}$ is the intermediate generated through the IRC path starting from $TS_{7,i,j}$; and $P_{7,i,j}$ corresponds to the IRC path through $TS_{7,i,j}$. The black, red, blue, and magenta lines indicate the path starting from most stable $A_{7,0,0}$ and three paths with lowest H_2 dissociation energy barrier, respectively. The other paths with higher TS energy are shown in gray colors. (b) Structures of $A_{7,0,0}$, $TS_{7,0,0}$, and $IM_{7,0,0}$, along $P_{7,0,0}$ starting from the most stable adsorption structure $A_{7,0,0}$. (c) Structures of $A_{7,i,j}$, $TS_{7,i,j}$, and $IM_{7,i,j}$, along paths with the three lowest barriers, $P_{7,0,1}$, $P_{7,1,0}$, $P_{7,1,1}$. In panels (b) and (c), relative free-energy values (in kJ/mol) are shown below the corresponding structures. Geometries and Cartesian coordinates for all these structures are shown in the Supporting Information.

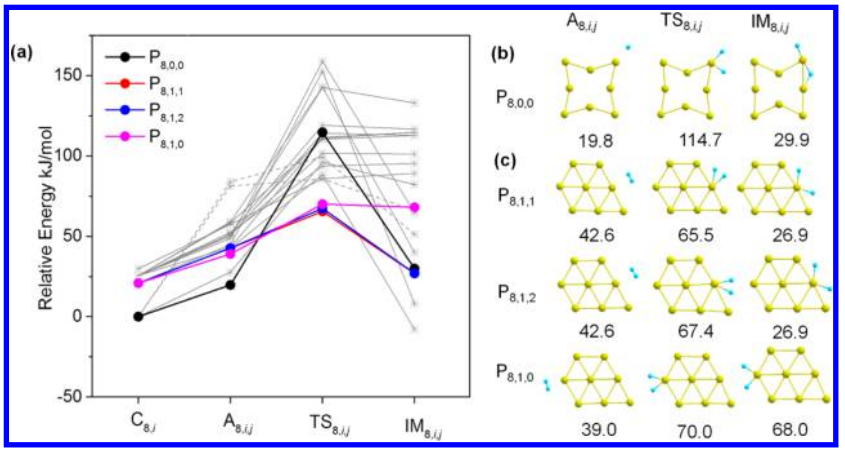

Figure 3. (a) Free-energy profiles (298.15 K, 1 atm) along 20 IRC paths for the H_2 dissociation step on the Au_8 clusters. Free-energy values are calculated relatively to $C_{8,0}$ + H_2. $A_{8,i,j}$ corresponds to the *j*th lowest adsorption state between $C_{8,i}$ and H_2; $TS_{8,i,j}$ is the TS for the IRC path connected to $A_{8,i,j}$; $IM_{8,i,j}$ is the intermediate generated through the IRC path starting from $TS_{8,i,j}$; and $P_{8,i,j}$ corresponds to the IRC path through $TS_{8,i,j}$. The black, red, blue, and magenta lines indicate the path starting from the most stable $A_{8,0,0}$ structure and three paths with the lowest H_2 dissociation energy barrier, respectively. The other paths with higher TS energy are shown in gray colors. Dashed lines indicate paths starting from $C_{8,0}$ + H_2 but have strong geometrical deviation in the Au_8 part at the adsorption structure, $A_{8,0,3}$ and $A_{8,0,4}$ (see the Supporting Information for their structures). (b) Structures of $A_{8,0,0}$, $TS_{8,0,0}$, and $IM_{8,0,0}$, along $P_{8,0,0}$ starting from the most stable adsorption structure $A_{8,0,0}$. (c) Structures of $A_{8,i,j}$, $TS_{8,i,j}$, and $IM_{8,i,j}$, along paths with the three lowest barriers, $P_{8,0,2}$, $P_{8,1,0}$, $P_{8,1,1}$. In panels (b) and (c), relative free energy values (in kJ/mol) are shown below the corresponding structures. Geometries and Cartesian coordinates for all these structures are shown in the Supporting Information.

lowest four, $C_{8,0}$, $C_{8,1}$, $C_{8,2}$, and $C_{8,3}$, are lying within the 20 kJ/mol energy range relative to the most stable structure, and hence, have been selected for further study, as was explained above. Dashed lines in Figure 3 indicate paths starting from $C_{8,0}$ + H_2 but having strong geometrical deviation in the Au_8 part at the adsorption structure, $A_{8,0,3}$ and $A_{8,0,4}$ (see the Supporting Information for their structures). A path starting from the fifth lowest $C_{8,4}$ structure has been also found as a result of the structural rearrangements in the course of path search by the AFIR method.

In the case of H_2 dissociation on Au_8 cluster, 20 different paths have been found. It is smaller than that observed for the Au_7 cluster, because the stable isomers of Au_8 have fewer reactive sites. The adsorption structures are energetically less favorable than the isolated Au_8 + H_2 state, because of entropy loss. Similar to the case of Au_7, the H_2 dissociation path starting from the lowest adsorption structure $A_{8,0,0}$ has a very high barrier, as shown in Figure 3b. In $A_{8,0,0}$, the H_2 binding energy $E^b_{8,0,0}$ is 14.2 kJ/mol, the Au−H distances are 2.01/2.01 Å, and the H−H distance is 0.79 Å. The H−H distance in $TS_{8,0,0}$ is 2.08 Å. Figure 3c shows three energetically favorable paths with the lowest TS energy. At $A_{8,1,1}$, $A_{8,1,2}$, and $A_{8,1,0}$, the H_2 binding energies $E^b_{8,1,1}$, $E^b_{8,1,2}$, and $E^b_{8,1,0}$ are 7.4, 7.4, and 12.4 kJ/mol, respectively, the Au−H distances are 2.19/2.20, 2.18/2.20, and

dx.doi.org/10.1021/ct500068b | J. Chem. Theory Comput. 2014, 10, 1623−1630

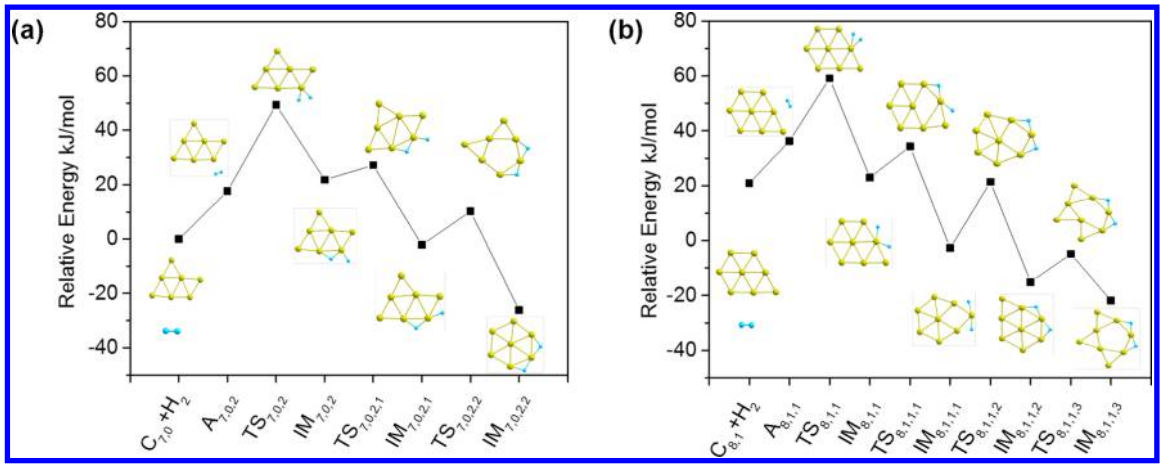

Figure 4. Full free-energy profiles (298.15 K, 1 atm) for the most favorable path of the H_2 dissociation reaction on the (a) Au_7 and (b) Au_8 clusters. $IM_{n,i,j,m}$ and $TS_{n,i,j,m}$ are intermediates and transition states, respectively, for the $(m+1)$-th reaction step of the most favorable H_2 dissociation path on Au_n.

1.96/1.96 Å, respectively, and the H−H distances are 0.78, 0.78, and 0.81 Å, respectively. $TS_{8,1,1}$, $TS_{8,1,2}$, and $TS_{8,1,0}$ have H−H distances of 1.16, 1.18, and 1.43 Å, respectively. Surprisingly, none of the three paths are associated with the most stable isomer $C_{8,0}$. Instead, all three preferable paths start from $C_{8,1}$, clearly demonstrating importance of accounting for the several isomeric structures for adequate description of the catalytic activity of gold clusters. Thus, in the case of Au_8, the second most stable isomer $C_{8,1}$ is the effective (actual) catalyst for the H_2 dissociation.

In order to confirm whether the Au_nH_2 clusters ($IM_{n,i,j}$) to reach the bottom of a local funnel of the H−Au_n−H type or to go back to H_2 + Au_n, further reaction pathways were followed in step (v) starting from the most favorable intermediates $IM_{7,0,2}$ and $IM_{8,1,1}$ to the lower energy isomers. Figure 4 shows the energy profiles calculated for the most favorable paths of the H_2 dissociation reaction on (a) Au_7 and (b) Au_8, respectively, starting from Au_n + H_2 to the stable form of Au_nH_2 clusters. Both $IM_{7,0,2}$ and $IM_{8,1,1}$ undergo further reaction steps toward stable forms $IM_{7,0,2,2}$ and $IM_{8,1,1,3}$, respectively, as seen in Figure 4. Although there are many other pathways and step (v) of the present searches actually located many pathways, showing only one in Figure 4 is enough to demonstrate that the H−H bond breaking is the rate-determining step and that going back to H_2 + Au_n from $IM_{n,i,j}$ is difficult.

3.1. Computational Cost. For Au_7 with γ = 300 kJ/mol, the number of gradient calculations (N_g) performed in steps (i)−(v) were 49180, 131492, 76972, 163659, and 39277, respectively. Figure 2a lists all pathways obtained by the search with γ = 300 kJ/mol. Among them, 9 paths possessing the lowest 9 TSs were located by the search with the smaller γ = 100 kJ/mol. In this γ = 100 kJ/mol search, N_g in steps (ii)−(iv) have been 34824, 10711, and 21350, respectively, where N_g for steps (i) and (v) does not depend on γ. Thus, the search with the smaller γ is much more efficient because high-lying paths are omitted. In this case, γ = 100 kJ/mol seems to be sufficient and a reasonable choice. For Au_8 with γ = 300 kJ/mol, N_g made in steps (i)−(v) have been 53583, 102066, 47890, 99038, and 49864, respectively. With γ = 100 kJ/mol, N_g performed in steps (ii)−(iv) have been reduced to 37862, 8960, and 15989, respectively. Moreover, 4 paths through the lowest 4 TSs were also found by the calculation with γ = 100 kJ/mol. Thus, the search with γ = 100 kJ/mol again is sufficient and an efficient choice for Au_8. Depending on the systems, some tests are recommended before deciding γ values not to overlook important pathways; choice of γ for other reactions are discussed in our previous publications.[51]

4. CONCLUSION

We proposed a systematic strategy for predicting the best single-bond activation path catalyzed by small metal clusters. The present approach has been successfully applied to the H_2 dissociation reaction on Au_7 and Au_8 clusters. Eleven (11) and 18 isomers were located for Au_7 and Au_8, respectively. The most stable isomers of Au_7 and Au_8 are planar, which are consistent with previous studies. Thirty three (33) and 20 transition state (TS) structures were found automatically for H_2 dissociation on Au_7 and Au_8 clusters, respectively, and successfully identified the best dissociation pathways with the lowest barrier. It was shown that stable adsorption structures do not necessarily related to low-energy TSs. Furthermore, we found that the most stable structures of gold clusters are not always the best catalysts at finite temperature. In the case of Au_7 cluster, the first two energetically low-lying isomeric structures contribute to the total reaction rate of H_2 dissociation. While for the Au_8 cluster, the second most stable isomer dominates the total reaction rate. The present results strongly suggest that systematic search for reaction pathways accounting for contribution of all low-energy isomers are required. Therefore, the proposed approach can serve as a promising tool for investigation of the chemical reactions catalyzed by small metal clusters.

■ ASSOCIATED CONTENT

Supporting Information

Cartesian coordinates for all these structures are available as Supporting Information. This material is available free of charge via the Internet at http://pubs.acs.org/.

■ AUTHOR INFORMATION

Corresponding Author

*E-mail: smaeda@mail.sci.hokudai.ac.jp.

Present Address

[§]On leave from V. A. Fock Institute of Physics, St. Petersburg State University, 198504 St. Petersburg, Petrodvorez, Russia.

Notes

The authors declare no competing financial interest.

■ ACKNOWLEDGMENTS

This work is partly supported by a grant from Japan Society for the Promotion of Science (Grants-in-Aid for Scientific Research ⟨KAKENHI⟩ No. 23685004 at Hokkaido University) and a grant from Japan Science and Technology Agency with Advanced Catalytic Transformation Program for Carbon Utilization (ACT-C) at Hokkaido University. Part of this work was performed under the management of the "Elements Strategy Initiative for Catalysts & Batteries (ESICB)" supported by the MEXT program "Elements Strategy Initiative to Form Core Research Center" (since 2012).

■ REFERENCES

(1) Landman, U.; Heiz, U. *Nanocatalysis*; Springer: Berlin, Heidelberg, New York, 2007.
(2) Corma, A.; Garcia, H. Supported gold nanoparticles as catalysts for organic reactions. *Chem. Soc. Rev.* **2008**, *37*, 2096−2126.
(3) Haruta, M. When gold is not noble: catalysis by nanoparticles. *Chem. Rec.* **2003**, *3*, 75−87.
(4) Hutchings, G. J.; Brust, M.; Schmidbaur, H. Gold—An introductory perspective. *Chem. Soc. Rev.* **2008**, *37*, 1759−1765.
(5) Tsunoyama, H.; Sakurai, H.; Tsukuda, T. Size effect on the catalysis of gold clusters dispersed in water for aerobic oxidation of alcohol. *Chem. Phys. Lett.* **2006**, *429*, 528−532.
(6) Haruta, M. Gold catalysts prepared by coprecipitation for low-temperature oxidation of hydrogen and of carbon monoxide. *J. Catal.* **1989**, *115*, 301−309.
(7) Haruta, M. Size- and support-dependency in the catalysis of gold. *Catal. Today* **1997**, *36*, 153−166.
(8) Haruta, M.; Kobayashi, T.; Sano, H.; Yamada, N. Novel gold catalysts for the oxidation of carbon monoxide at a temperature far below 0 °C. *Chem. Lett.* **1987**, *16*, 405−408.
(9) Min, B. K.; Friend, C. M. Heterogeneous gold-based catalysis for green chemistry: Low-temperature CO oxidation and propene oxidation. *Chem. Rev.* **2007**, *107*, 2709−2724.
(10) Häkkinen, H.; Landman, U. Gold clusters (Au_N, $2 \le N \le 10$) and their anions. *Phys. Rev. B* **2000**, *62*, R2287−R2290.
(11) Olson, R. M.; Varganov, S.; Gordon, M. S.; Metiu, H.; Chretien, S.; Piecuch, P.; Kowalski, K.; Kucharski, S. A.; Musial, M. Where does the planar-to-nonplanar turnover occur in small gold clusters? *J. Am. Chem. Soc.* **2005**, *127*, 1049−1052.
(12) Häkkinen, H. Atomic and electronic structure of gold clusters: Understanding flakes, cages and superatoms from simple concepts. *Chem. Soc. Rev.* **2008**, *37*, 1847−1859.
(13) Sánchez-Portal, D.; Artacho, E.; Junquera, J.; Ordejón, P.; García, A.; Soler, J. M. Stiff monatomic gold wires with a spinning zigzag geometry. *Phys. Rev. Lett.* **1999**, *83*, 3884−3887.
(14) Djalali, R.; Li, S.-Y.; Schmidt, M. Amphipolar core-shell cylindrical brushes as templates for the formation of gold clusters and nanowires. *Macromolecules* **2002**, *35*, 4282−4288.
(15) Garzón, I. L.; Michaelian, K.; Beltrán, M. R.; Posada-Amarillas, A.; Ordejón, P.; Artacho, E.; Sánchez-Portal, D.; Soler, J. M. Lowest energy structures of gold nanoclusters. *Phys. Rev. Lett.* **1998**, *81*, 1600−1603.
(16) Michaelian, K.; Rendón, N.; Garzón, I. L. Structure and energetics of Ni, Ag, and Au nanoclusters. *Phys. Rev. B* **1999**, *60*, 2000−2010.
(17) Rossi, G.; Ferrando, R.; Rapallo, A.; Fortunelli, A.; Curley, B. C.; Lloyd, L. D.; Johnston, R. L. Global optimization of bimetallic cluster structures. II. Size-matched Ag−Pd, Ag−Au, and Pd−Pt systems. *J. Chem. Phys.* **2005**, *122*, 194309/1−194309/9.
(18) Pyykkö, P. Theoretical chemistry of gold. *Angew. Chem., Int. Ed.* **2004**, *43*, 4412−4456.
(19) Sanchez, A.; Abbet, S.; Heiz, U.; Schneider, W. D.; Häkkinen, H.; Barnett, R. N.; Landman, U. When gold is not noble: Nanoscale gold catalysts. *J. Phys. Chem. A* **1999**, *103*, 9573−9578.
(20) Gao, M.; Lyalin, A.; Taketsugu, T. CO oxidation on h-BN supported Au atom. *J. Chem. Phys.* **2013**, *138*, 034701/1−034701/8.
(21) Lopez, N.; Janssens, T. V. W.; Clausen, B. S.; Xu, Y.; Mavrikakis, M.; Bligaard, T.; Nørskov, J. K. On the origin of the catalytic activity of gold nanoparticles for low-temperature CO oxidation. *J. Catal.* **2004**, *223*, 232−235.
(22) Gao, M.; Lyalin, A.; Taketsugu, T. Oxygen activation and dissociation on h-BN supported Au atoms. *Int. J. Quantum Chem.* **2013**, *113*, 443−452.
(23) Molina, L. M.; Hammer, B. Some recent theoretical advances in the understanding of the catalytic activity of Au. *Appl. Catal., A* **2005**, *291*, 21−31.
(24) Hansen, J. A.; Ehara, M.; Piecuch, P. Aerobic oxidation of methanol to formic acid on Au_8^-: Benchmark analysis based on completely renormalized coupled-cluster and density functional theory calculations. *J. Phys. Chem. A* **2013**, *117*, 10426−10427.
(25) Okumura, M.; Kitagawa, Y.; Haruta, M.; Yamaguchi, K. The interaction of neutral and charged Au clusters with O_2, CO and H_2. *Appl. Catal., A* **2005**, *291*, 37−44.
(26) Barrio, L.; Liu, P.; Rodriguez, J. A.; Campos-Martin, J. M.; Fierro, J. L. G. A density functional theory study of the dissociation of H_2 on gold clusters: importance of fluxionality and ensemble effects. *J. Chem. Phys.* **2006**, *125*, 164715/1−164715/5.
(27) Boronat, M.; Illas, F.; Corma, A. Active sites for H_2 adsorption and activation in Au/TiO_2 and the role of the support. *J. Phys. Chem. A* **2009**, *113*, 3750−3757.
(28) Fujitani, T.; Nakamura, I.; Akita, T.; Okumura, M.; Haruta, M. Hydrogen dissociation by gold clusters. *Angew. Chem., Int. Ed.* **2009**, *48*, 9515−9518.
(29) Lyalin, A.; Taketsugu, T. A computational investigation of H_2 adsorption and dissociation on Au nanoparticles supported on TiO_2 surface. *Faraday Discuss.* **2011**, *152*, 185−201.
(30) Zanchet, A.; Dorta-Urra, A.; Aguado, A.; Roncero, O. Understanding structure, size, and charge effects for the H_2 dissociation mechanism on planar gold clusters. *J. Phys. Chem. C* **2011**, *115*, 47−57.
(31) Joshi, A.; Delgass, W. N.; Thomson, K. T. H_2 adsorption and H/D exchange on Au/TS-1 and Au/S-1 catalysts. *Top. Catal.* **2007**, *44*, 27−39.
(32) Gruene, P.; Rayner, D. M.; Redlich, B.; van der Meer, A. F. G.; Lyon, J. T.; Meijer, G.; Fielicke, A. Structures of neutral Au_7, Au_{19}, and Au_{20} clusters in the gas phase. *Science* **2008**, *321*, 674−676.
(33) Vargas, A.; Santarossa, G.; Iannuzzi, M.; Baiker, A. Fluxionality of gold nanoparticles investigated by Born−Oppenheimer molecular dynamics. *Phys. Rev. B* **2009**, *80*, 195421/1−195421/13.
(34) Arenz, M.; Landman, U.; Heiz, U. CO combustion on supported gold clusters. *ChemPhysChem* **2006**, *7*, 1871−1879.
(35) Koskinen, P.; Häkkinen, H.; Huber, B.; von Issendorff, B.; Moseler, M. Liquid−liquid phase coexistence in gold clusters: 2D or not 2D? *Phys. Rev. Lett.* **2007**, *98*, 015701/1−015701/4.
(36) Gu, X.; Bulusu, S.; Li, X.; Zeng, X. C.; Li, J.; Gong, X. G.; Wang, L.-S. Au_{34}^-: A fluxional core-shell cluster. *J. Phys. Chem. C* **2007**, *111*, 8228−8232.
(37) Li, Z. Y.; Young, N. P.; Di Vece, M.; Palomba, S.; Palmer, R. E.; Bleloch, A. L.; Curley, B. C.; Johnston, R. L.; Jiang, J.; Yuan, J. Three-dimensional atomic-scale structure of size-selected gold nanoclusters. *Nature* **2008**, *451*, 46−48.
(38) Wales, D. J.; Scheraga, H. A. Global optimization of clusters, crystals, and biomolecules. *Science* **1999**, *285*, 1368−1372.
(39) Heiles, S.; Johnston, R. L. Global optimization of clusters using electronic structure methods. *Int. J. Quantum Chem.* **2013**, *113*, 2091−2109.
(40) Schlegel, H. B. Exploring potential energy surfaces for chemical reactions: An overview of some practical methods. *J. Comput. Chem.* **2003**, *24*, 1514−1527.

(41) Wales, D. J. Energy landscapes: Calculating pathways and rates. *Int. Rev. Phys. Chem.* **2006**, *25*, 237−282.
(42) Jensen, F. Optimization techniques. *Introduction to Computational Chemistry*, 2nd ed.; Wiley: Chichester, U.K., 2007; pp 380−420.
(43) Schlegel, H. B. Geometry optimization. *WIREs Comput. Mol. Sci.* **2011**, *1*, 790−809.
(44) Abashkin, Y.; Russo, N. Transition state structures and reaction profiles from constrained optimization procedure. Implementation in the framework of density functional theory. *J. Chem. Phys.* **1994**, *100*, 4477−4483.
(45) Bondensgård, K.; Jensen, F. Gradient extremal bifurcation and turning points: an application to the H_2CO potential energy surface. *J. Chem. Phys.* **1996**, *104*, 8025−8031.
(46) Quapp, W.; Hirsch, M.; Imig, O.; Heidrich, D. Searching for saddle points of potential energy surfaces by following a reduced gradient. *J. Comput. Chem.* **1998**, *19*, 1087−1100.
(47) Černohorský, M.; Kettou, S.; Koča, J. *VADER*: New software for exploring interconversions on potential energy surfaces. *J. Chem. Inf. Comput. Sci.* **1999**, *39*, 705−712.
(48) Irikura, K. K.; Johnson, R. D., III. Predicting unexpected chemical reactions by isopotential searching. *J. Phys. Chem. A* **2000**, *104*, 2191−2194.
(49) Müller, E. M.; de Meijere, A.; Grubmüller, H. Predicting unimolecular chemical reactions: Chemical flooding. *J. Chem. Phys.* **2002**, *116*, 897−905.
(50) Zimmerman, P. M. Automated discovery of chemically reasonable elementary reaction steps. *J. Comput. Chem.* **2013**, *34*, 1385−1392.
(51) Maeda, S.; Ohno, K.; Morokuma, K. Systematic exploration of the mechanism of chemical reactions: The global reaction route mapping (GRRM) strategy using the ADDF and AFIR methods. *Phys. Chem. Chem. Phys.* **2013**, *15*, 3683−3701.
(52) Ohno, K.; Maeda, S. A scaled hypersphere search method for the topography of reaction pathways on the potential energy surface. *Chem. Phys. Lett.* **2004**, *384*, 277−282.
(53) Ohno, K.; Maeda, S. Global reaction route mapping on potential energy surfaces of formaldehyde, formic acid, and their metal-substituted analogues. *J. Phys. Chem. A* **2006**, *110*, 8933−8941.
(54) Maeda, S.; Ohno, K. Global Mapping of equilibrium and transition structures on potential energy surfaces by the scaled hypersphere search method: Applications to *ab initio* surfaces of formaldehyde and propyne molecules. *J. Phys. Chem. A* **2005**, *109*, 5742−5753.
(55) Maeda, S.; Morokuma, K. Communications: A systematic method for locating transition structures of A+B→X type reactions. *J. Chem. Phys.* **2010**, *132*, 241102/1−241102/4.
(56) Maeda, S.; Morokuma, K. Finding reaction pathways of type A +B→X: Toward systematic prediction of reaction mechanisms. *J. Chem. Theory Comput.* **2011**, *7*, 2335−2345.
(57) Fukui, K. The path of chemical-reactions—The IRC approach. *Acc. Chem. Res.* **1981**, *14*, 363−368.
(58) Choi, C.; Elber, R. Reaction path study of helix formation in tetrapeptides: effect of side chains. *J. Chem. Phys.* **1991**, *94*, 751−760.
(59) Banerjee, A.; Adams, N.; Simons, J.; Shepard, R. Search for stationary points on surfaces. *J. Phys. Chem.* **1985**, *89*, 52−57.
(60) Maeda, S.; Ohno, K. Structures of water octamers $(H_2O)_8$: Exploration on *ab initio* potential energy surfaces by the scaled hypersphere search method. *J. Phys. Chem. A* **2007**, *111*, 4527−4534.
(61) Earl, D. J.; Deem, M. W. Parallel tempering: Theory, applications and new perspectives. *Phys. Chem. Chem. Phys.* **2005**, *7*, 3910−3916.
(62) Page, M.; McIver, J. W., Jr. On evaluating the reaction path Hamiltonian. *J. Chem. Phys.* **1988**, *88*, 922−935.
(63) Perdew, J. P.; Burke, K.; Ernzerhof, M. Generalized gradient approximation made simple. *Phys. Rev. Lett.* **1996**, *77*, 3865−3868.
(64) Sánchez-Portal, D.; Ordejón, P.; Artacho, E.; Soler, J. M. Density-functional method for very large systems with LCAO basis sets. *Int. J. Quantum Chem.* **1997**, *65*, 453−461.
(65) Soler, J. M.; Artacho, E.; Gale, J. D.; García, A.; Junquera, J.; Ordejón, P.; Sánchez-Portal, D. The SIESTA method for *ab initio* order-*N* materials simulation. *J. Phys.: Condens. Matter.* **2002**, *14*, 2745.
(66) Sánchez-Portal, D.; Ordejón, P.; Canadell, E. Computing the properties of materials from first principles with SIESTA. In *Principles and Applications of Density Functional Theory in Inorganic Chemistry II*; Springer: Berlin, Heidelberg, 2004; Vol. *113*, pp 103−170.
(67) Serapian, S. A.; Bearpark, M. J.; Bresme, F. The shape of Au_8: Gold leaf or gold nugget? *Nanoscale* **2013**, *5*, 6445−6457.
(68) Junquera, J.; Paz, Ó.; Sánchez-Portal, D.; Artacho, E. Numerical atomic orbitals for linear-scaling calculations. *Phys. Rev. B* **2001**, *64*, 235111/1−235111/9.
(69) Troullier, N.; Martins, J. L. Efficient pseudopotentials for plane-wave calculations. *Phys. Rev. B* **1991**, *43*, 1993−2006.
(70) Assadollahzadeh, B.; Schwerdtfeger, P. A systematic search for minimum structures of small gold clusters Au_n (n = 2 - 20) and their electronic properties. *J. Chem. Phys.* **2009**, *131*, 064306/1−064306/11.
(71) Remacle, F.; Kryachko, E. S. Structure and energetics of two- and three-dimensional netural, cationic, and anionic gold clusters $Au^z_{5\le n\le 9}$ (Z = 0, ±1). *J. Chem. Phys.* **2005**, *122*, 04434/1−04434/14.
(72) Xiao, L.; Wang, L. From planar to three-dimensional structural transition in gold clusters and the spin-orbit coupling effect. *Chem. Phys. Lett.* **2004**, *392*, 452−455.
(73) Li, X.-B.; Wang, H.-Y.; Yang, X.-D.; Zhu, Z.-H.; Tang, Y.-J. Size dependence of the structures and energetic and electronic properties of gold clusters. *J. Chem. Phys.* **2007**, *126*, 084505/1−084505/8.
(74) Diefenbach, M.; Kim, K. S. Spatial Structure of Au_8: importance of basis set completeness and geometry relaxation. *J. Phys. Chem. B* **2006**, *110*, 21639−21642.
(75) Han, Y.-K. Structure of Au_8: Planar or nonplanar? *J. Chem. Phys.* **2006**, *124*, 024316/1−024316/3.
(76) Hansen, J. A.; Piecuch, P.; Levine, B. G. Communication: determining the lowest-energy isomer of Au_8: 2D, or not 2D. *J. Chem. Phys.* **2013**, *139*, 091101/1−091101/4.
(77) Martínez, A. Size matters, but is being planar of any relevance? Electron donor-acceptor properties of neutral gold clusters up to 20 atoms. *J. Phys. Chem. C* **2010**, *114*, 21240−21246.